2.5 - D Finite Element Algorithm for MCSEM Modeling.

Luiz Rijo, UFPA, Brazil
rijo@amazon.com.br

This paper was prepared for presentation at the 9th International Congress of the Brazilian Geophysical Society held in Salvador, Brazil, 11-14 September 2005.

Abstract

Recently a new and very important geophysical method for detection of oil-filled reservoir in deep-water areas has been introducing in the petroleum industry. The method, called Marine Controlled Source Electromagnetic (MCSEM), also known as Sea Bed Logging (SBL), maps the contrast between the electrical resistivity of an oil-filled reservoir and that of the sedimentary host strata. Usually the resistivity of the former is greater than that of the latter. The MCSEM method is based on the diffusion of electromagnetic energy at low frequency generated by a mobile horizontal electrical dipole and detected by an array of receivers distributed on seafloor. In this paper we present a finite element algorithm for 2.5-D MCSEM modeling. The performance of the algorithm is illustrated by means of some selected examples.

Introduction

In the last few years, a new geophysical method called MCSEM (Marine Controlled - Source Electromagnetic), also known as SBL (Sea Bed Logging) destined for petroleum exploration in deep waters has drawn attention of several oil companies. The MCSEM method is based on the use of a mobile horizontal electric dipole (HED) source and an array of electric field receivers distributed on the seafloor (Eidesmo et al., 2002). The transmitting dipole emits a low frequency (0.125 to 2 Hz) signal that diffuses outwards both into the overlying water layer and downwards into the seabed sediments. The receivers at the seafloor give the amplitude and phase of the electric field signal, which depends on both the geometry and the resistivity of the underlying sediments. The method relies on the moderate resistivity contrast between oil-saturated reservoirs and the surrounding sedimentary layers saturated with aqueous saline fluids. International contractor geophysical companies specialized in this technology have being busy carried out surveys in many part of the world, including here in Brazil. Research at universities supported by oil-companies, like de CEMI coordinated by Zhadanov at University of Utah and the Script Institution of Oceanography, San Diego, CA. consortium coordinate by Constable, has help clarify the pit-falls behind this method. In this paper we present same interesting results based on a finite element algorithm for 2.5-D MCSEM modeling.

Methodology

In view of the geometry of the HED the MCSEM modeling is essentially a three-dimensional electromagnetic problem. However, if the length of the reservoir in one horizontal direction is much larger than in the other two directions the problem can be treaded mathematically as a sequence of two-dimensional partial problems. This can be accomplished by Fourier transformation (Stoyer & Greenfield, 1976; Unsworth at a., 1993) with respect to the strike direction, for example y-axis. This methodology is known as 2.5-D modeling. Each partial two-dimensional problem can easily be solved by the finite element method in term of secondary field components E_y and H_y, where y is the strike of the 2-D reservoir. Technically these two components are coupled into TE and TM electromagnetic modes. The Ex and E_z components are obtained from E_y and H_y by numerical derivatives. The final approximate solution of the secondary electrical field is obtained via inverse Fourier transform from all these 2-D partial problems. For that we used the linear digital filter technique with 30 coefficients for the sine and co-sine filters (Rijo & Almeida, 2003). Finally, this approximated secondary solution is added to the primary solution which is solved analytically by the Hankel transforms J_0 and J_1. These transforms were computed with the system *Mathematica*. See the Appendix for more details about the algoritm.

Examples

The model used for illustrating the performance of our algorithm is shown in the Figure 1, suggested by Marco Polo from Petrobras. The thickness of the seawater layer is h_1 = 1500 m with the seawater resistivity equal to 0.3 ohm-m. The resistivity of the oil-filled reservoir is 10 ohm-m with h_3 = 50 m thickness at h_2 = 950 m below the sea bottom. The resistivity of the host sediments is 0.8 ohm-m. The HED is 30 m above the sea floor. The frequency used in the transmitter is equal to 0.125 Hz. The lateral extensions of the reservoir are 3, 5, 7 and 10 km. Initially, the in-line responses of E_x and E_z components of the electric field are shown. Afterwards, the maps of these components at the sea bottom covering an area of 15 km X 15 km around the transmitter with 60 X 60 receivers are discussed.

In-line responses

In order to facilitate the comprehension of the 2.5-D responses it is useful to have the 1-D response for comparison. In Figure 2 the red curve corresponds the amplitude of the E_x electrical component of the background model (half-space), that is, the model without

the reservoir. The magenta curve is the response of the 1-D model. Yellow, green, cyan and blue curves correspond to the responses of the 3, 5, 7 and 10 km reservoirs, respectively. Note that these are noise free data. Real data is commonly noisy, therefore it is difficult, based on this kind of information, to tell if the reservoir is 1-D or 2.5-D.

depending on the lateral extension (3 km to 10 km) of the reservoir.

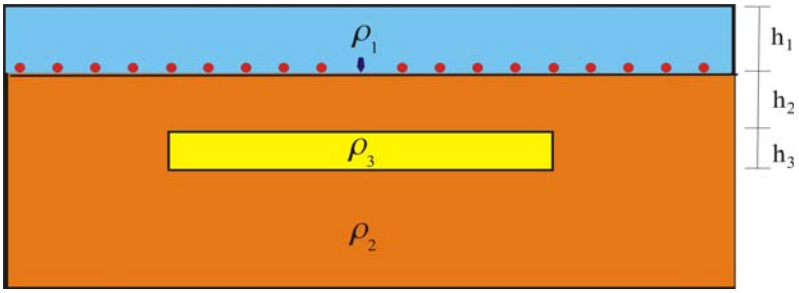

Figure 1. The yellow rectangle represents the cross XZ section the oil-filled reservoir. The blue arrow represents the transmitter and the red points the receivers.

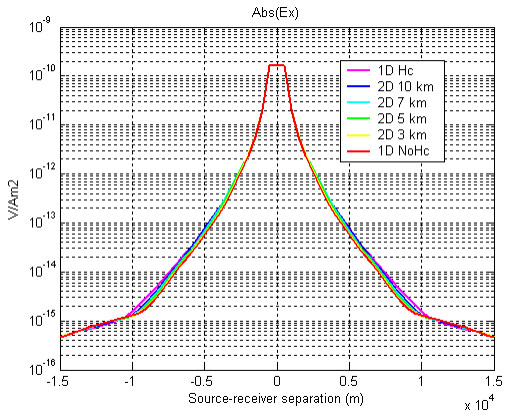

Figure 2. Comparison of the 1-D (magenta) and 2.5-D E_x amplitude responses. The red curve is associated with the background model, that is, the half-spece without hydrocarbon (NoHc).

The phase of the E_x response are shown in Figure 3. It is still difficult to discriminate the 2.5-D models from the 1-D model.

In order to highlight the effect on the response of the reservoir it is a common practice to normalize the E_x field strengths by that of the corresponding background model. (Eidesmo et al., 2002). The normalized E_x responses of the 1-D and 2.5-D models are shown in Figure 4. Now, we can easily visualize the effect on the E_x response of all models. Indeed, the anomalies very from 10% to 40%

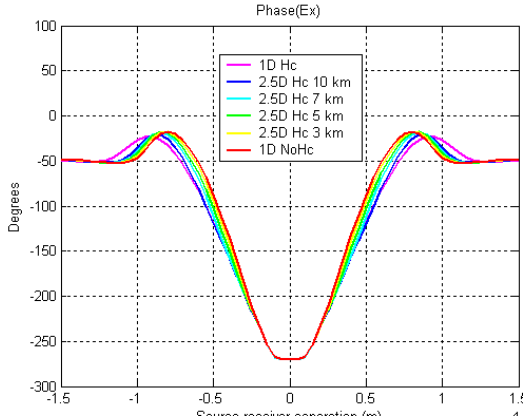

Figure 3. Comparison of the 1-D (magenta) with 2.5-D E_x phase response. The red curve is associated with the background model

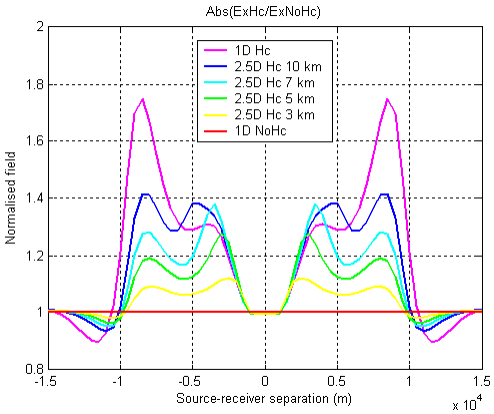

Figure 4. Normalized E_x field strengths by the corresponding background model.

The next three figures shown similar results for the E_z field components. Figure 5 shown the amplitude and Figure 6 the phase of the E_z field. Based on these results there is no much difference between the strengths of E_x and E_z electric field components.

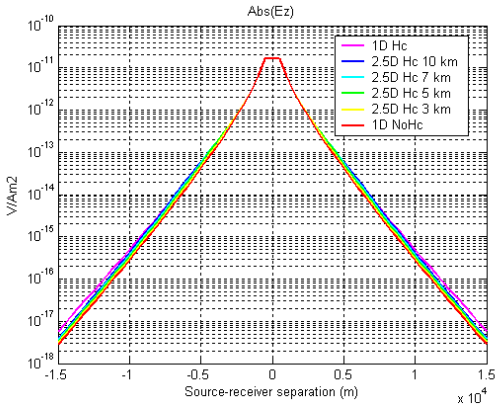

Figure 5. Comparison of the 1-D (magenta) and 2.5-D E_x amplitude responses

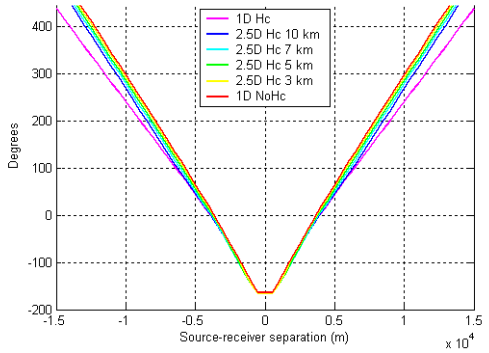

Figure 6. Comparison of the 1-D (magenta) and 2.5-D E_z phase responses

The normalized field strengths are show in Figure 7. Here, the anomalies very from 10% to 60% according to the lateral extension of the reservoir.

Maps of normalized fields

Due to the three-dimensional character of the HED source, a single in-line profile is not enough to reveal the complete picture of MCSEM anomalies even in the 1-D case. Indeed, the Figure 8 shows a map of the normalized field for the 1-D reservoir. The map shows a typical dipole pattern with four lobes symmetrically distributed. The E_x strength at the center of each lobe is

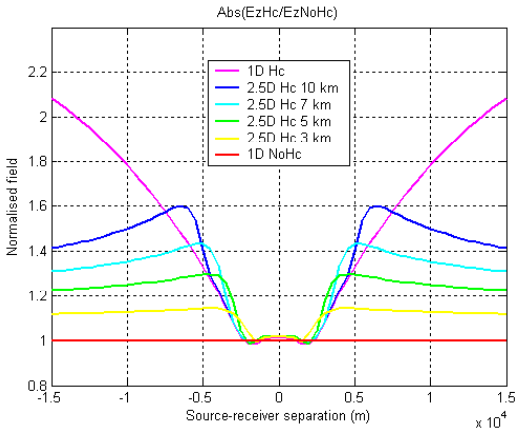

Figure 7. Normalized E_z field strengths by the corresponding background model.

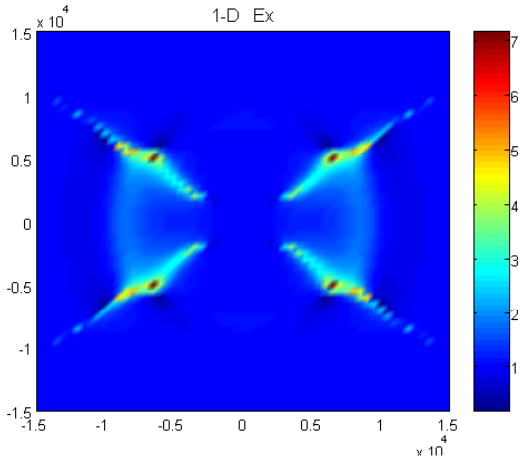

Figure 8. Map of the normalized E_x strengths of the 1-D model

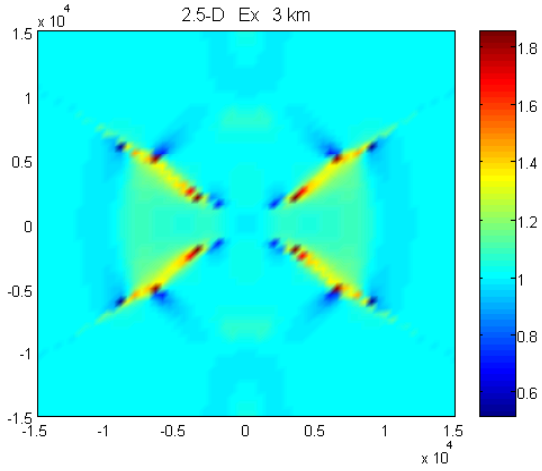

Figure 9. Map of the normalized E_x strengths of the 3.5-D 3 km model

A similar dipole pattern characterizes the map of the 3 km 2-D reservoir as illustrated in Figure 9. The four lobes are practically at the same position in despite of small extension of the reservoir in one direction. However, the field strength in the center of each lobe is only 80% of field intensity of the background model. Figures 10 and 11 and 12 show the maps of the 5, 7 and 10 km reservoirs. The dipole pattern in each map is absolutely the same as before.

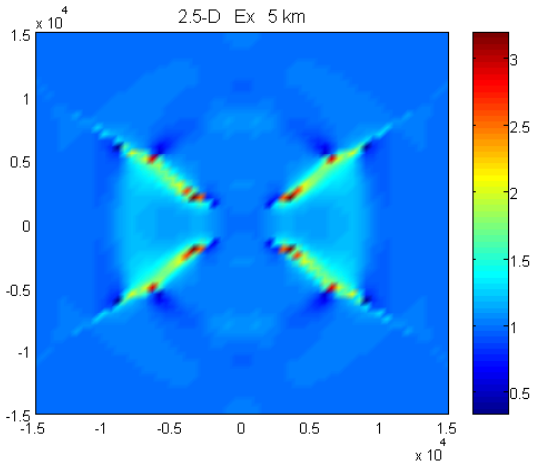

Figure 10. Map of the normalized E_x strengths of the 2.5-D 5 km model

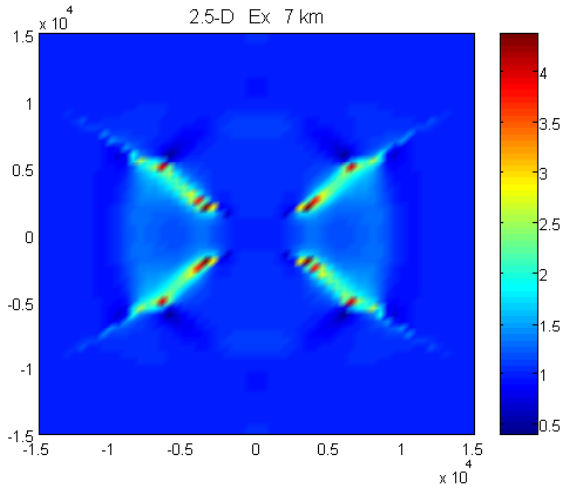

Figure 11. Map of the normalized E_x strengths of the 2.5-D 7 km model

The map of the normalized 1-D E_z component has a radial pattern centered at the dipole transmitter as shown in Figure 13. The intensity of the normalized E_z increases gradually from the center in all directions up to 100%. Identical pattern are observed in the case of 2.5-D models. The anomaly increases radially outwards from the center of the electric horizontal dipole. The normalized field strength reaches 13% (3 km), 22% (5 km), 30% (7 km) and 40% (10 km) according to the lateral extension of the 2-D reservoir.

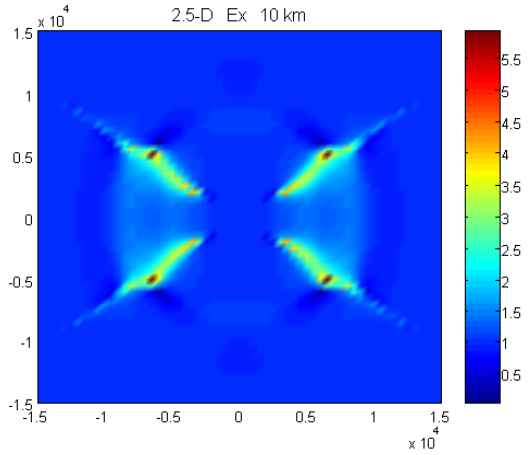

Figure 12. Map of the normalized E_x strengths of the 2.5-D 10 km model

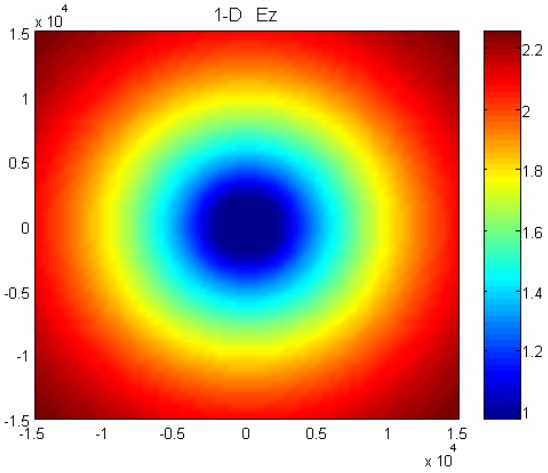

Figure 13. Map of the normalized E_z strengths of the 1-D model

Conclusions

MCSEM (Marine Controlled Source Electromagnetic) is a new geophysical technology for mapping resistive layers associated with oil-filled reservoir. This geophysical method opens new horizon for petroleum exploration in deep-water areas. Complemented with MMT (Marine Magnetotelluric) this new geophysical method will certainly contribute for minimizing the exploration risk. We saw in this paper that the MCSEM method is effective even for very low resistivity contrast between the conductive host sediments (0.8 ohm-m) and the moderate resistive reservoir (10 ohm m). The finite element method algorithm presented here is very powerful methodology for modeling 2.5-D MCSEM data. The modeling of E_x and E_z in-line profiles data takes approximately 3 min on a

Pentium IV PC. A complete map with 40 parallel profiles takes 2 hours in the same computer.

Acknowledgments

The author acknowledges the support of Petrobrás (Contract Petrobras/Fadesp/UFPA 6502282033) for this project. Also, he acknowledges the ANP PRH-06 for his PV fellowship and for supporting the PROEM Laboratory. Especial thanks are given to Dr. Marco Polo from Petrobras for many hours of fruitful discussion on MCSEM method.

References

EIDESMO, T., ELLINGSRUD, S., MACGREGOR , L. M., CONSTABLE, SINHA, M. C., JOHANSEN, S., KONG, F. N. and WESTERDAHL, H., 2002. Sea Bed Logging (SBL), a new method for remote and direct identification of hydrocarbon filled layers in deepwater areas: First Break, 20, 144 – 152.

RIJO L. & ALMEIDA, F. L., 2003. New optimized digital filters for sine co-sine, J_0 and J_1 Hankel transforms. In: 8th International Congress of Brazilian Geophysical Society. Rio de Janeiro, SBGF. In CD-ROM.

STOYER, C. H. & GREENFIELD, R. J., 1976, Numerical Solution of the response of a two-dimensional earth to an oscillating magnetic dipole source: Geophysics, 41, 519-530.

UNSWORTH, M. J., TRAVIS, B. J. CHAVE, A. D., 1993, Electromagnetic induction by a finite electric dipole over a 2-dimemsional earth. Geophysics, 58, 198-214.

Appendix

The Galerkin finite element formulation for 2.5-D low-frequency EM problems, in SI units, is given by the following coupled integrals

$$\int_{\omega^e}\psi_i\left[-\frac{\partial}{\partial x}\left(\frac{\sigma}{u^2}\frac{\partial\hat{E}_y^s}{\partial x}\right)+\sigma\hat{E}_y^s-\frac{\partial}{\partial z}\left(\frac{\sigma}{u^2}\frac{\partial\hat{E}_y^s}{\partial z}\right)\right]dxdz$$
$$+\int_{\omega^e}\psi_i\left[-\frac{\partial}{\partial x}\left(\frac{ik_y}{u^2}\frac{\partial H_y^s}{\partial z}\right)+\frac{\partial}{\partial z}\left(\frac{ik_y}{u^2}\frac{\partial H_y^s}{\partial x}\right)\right]dxdz$$
$$=\int_{\omega^e}\psi_i\left[\frac{\partial}{\partial x}\left(\frac{ik_y\Delta\sigma}{u^2}\hat{E}_x^p\right)-\Delta\sigma\hat{E}_y^p+\frac{\partial}{\partial z}\left(\frac{ik_y\Delta\sigma}{u^2}\hat{E}_z^p\right)\right]dxdz$$

and

$$\int_{\omega^e}\psi_i\left[\frac{\partial}{\partial x}\left(\frac{ik_y}{u^2}\frac{\partial\hat{E}_y^s}{\partial z}\right)-\frac{\partial}{\partial z}\left(\frac{ik_y}{u^2}\frac{\partial\hat{E}_y^s}{\partial x}\right)\right]dxdz$$
$$+\int_{\omega^e}\psi_i\left[-\frac{\partial}{\partial x}\left(\frac{i\omega\mu_0}{u^2}\frac{\partial H_y^s}{\partial x}\right)+i\omega\mu_0 H_y^s-\frac{\partial}{\partial z}\left(\frac{i\omega\mu_0}{u^2}\frac{\partial H_y^s}{\partial z}\right)\right]dxdz$$
$$=\int_{\omega^e}\psi_i\left[\frac{\partial}{\partial z}\left(\frac{i\omega\mu_0\Delta\sigma}{u^2}\hat{E}_x^p\right)-\frac{\partial}{\partial x}\left(\frac{i\omega\mu_0\Delta\sigma}{u^2}\hat{E}_z^p\right)\right]dxdz$$

where ψ_i (i = 1, N) are the linear basis functions, E_y^s and H_y^s are the Fourier transform of the secondary y components of the electric and magnetic fields and u^2 is the squared of the propagation constant expressed by

$$u^2 = k_x^2 + k_y^2 + i\omega\mu_0\sigma$$

The Fourier transform of the E_x, E_y and E_z components of the primary electric field (in the layering half-space) on the right-hand side integrals are given by

$$E_x^p(x,k_y,z) = -\frac{\rho_2 Ids}{4\pi}\int_{-\infty}^{\infty}u_2 K_{TM}(k_x,k_y,z)\frac{k_x^2}{k_x^2+k_y^2}e^{ik_x x}dk_x$$
$$-\frac{\rho_1 Ids}{4\pi}\int_{-\infty}^{\infty}\frac{2i}{u_1}K_{TE}(k_x,k_y,z)\frac{k_y^2}{k_x^2+k_y^2}e^{ik_x x}dk_x$$

$$E_y^p(x,k_y,z) = -\frac{\rho_2 Ids}{4\pi}\int_{-\infty}^{\infty}u_2 K_{TM}(k_x,k_y,z)\frac{k_x k_y}{k_x^2+k_y^2}e^{ik_x x}dk_x$$
$$+\frac{\rho_1 Ids}{4\pi}\int_{-\infty}^{\infty}\frac{2i}{u_1}K_{TE}(k_x,k_y,z)\frac{k_x k_y}{k_x^2+k_y^2}e^{ik_x x}dk_x$$

$$E_z^p(k_x,k_y,z) = -\frac{\rho_2 Ids}{4\pi}\int_{-\infty}^{\infty}ik_x K_{TM}(k_x,k_y,z)e^{ik_x x}dk_x$$

The functions K_{TE} and K_{TM} in these integrals have geometric and electric properties information about the primary model.

Now, applying integration-by-part (second Green identity) in the above Galerkin finite element integrals yields

$$\frac{\sigma_e}{u_e^2}\int_{\Omega_e}\left(\frac{\partial\psi_m}{\partial x}\frac{\partial\hat{E}_y^s}{\partial x}+\frac{\partial\psi_m}{\partial z}\frac{\partial\hat{E}_y^s}{\partial z}\right)dxdz$$
$$+\sigma_e\int_{\Omega_e}\psi_m\hat{E}_y^s dxdz$$
$$+\frac{ik_e}{u_e^2}\int_{\Omega_e}\left(\frac{\partial\psi_m}{\partial x}\frac{\partial H_y^s}{\partial z}-\frac{\partial\psi_m}{\partial z}\frac{\partial H_y^s}{\partial x}\right)dxdz$$
$$=-\frac{ik_y\Delta\sigma_e}{u_e^2}\int_{\Omega_e}\left[\frac{\partial\psi_m}{\partial x}\hat{E}_x^p+\frac{\partial\psi_m}{\partial z}\hat{E}_z^p\right]dxdz$$
$$-\Delta\sigma_e\int_{\Omega_e}\psi_m\hat{E}_y^p dxdz$$
$$-\int_{\partial\Omega_e}\psi_m H_x^s dx+\psi_m H_z^s dz$$

and

$$
\begin{aligned}
&-\frac{ik_e}{u_e^2}\int_{\Omega_e}\left(\frac{\partial\psi_m}{\partial x}\frac{\partial\hat{E}_y^s}{\partial z}-\frac{\partial\psi_m}{\partial z}\frac{\partial\hat{E}_y^s}{\partial x}\right)dxdz\\
&+\frac{i\omega\mu_0}{u_e^2}\int_{\Omega_e}\left(\frac{\partial\psi_m}{\partial x}\frac{\partial H_y^s}{\partial x}+\frac{\partial\psi_m}{\partial z}\frac{\partial H_y^s}{\partial z}\right)dxdz\\
&+i\omega\mu_0\int_{\Omega_e}\psi_m H_y^s dxdz\\
=&-\frac{i\omega\mu_0\Delta\sigma}{u_e^2}\int_{\Omega_e}\left[\frac{\partial\psi_m}{\partial z}\hat{E}_x^p-\frac{\partial\psi_m}{\partial x}\hat{E}_z^p\right]dxdz\\
&+\int_{\partial\omega^e}\psi_m\hat{E}_x^p dx+\psi_m\hat{E}_z^p dz
\end{aligned}
$$

Assuming

$$E_y^s=\sum_{i=1}^{N}E_i\psi_i \qquad H_y^s=\sum_{i=1}^{N}H_i\psi_i$$

in each element and substituting into the above integrals, we obtain the element matrix of each cell of the finite element mesh. We used triangular elements, thus the element matrix is 6x6. These element matrices are assembled to form a sparse banded system of linear equations. In the internal elements the line integrals cancel out due to the continuity of the tangential components of the electric and magnetic fields and of the basis functions as well. On the external elements (those on the boundary of the mesh) these integrals do not need to be computed because the homogeneous Dirichlet boundary conditions on the contour of the mesh. After solving the global system of linear equations for the secondary E_y and H_y components we compute numerically the secondary E_x and E_z components using the following expressions

$$\hat{E}_x^s=-\left(\frac{ik_y}{u^2}\frac{\partial\hat{E}_y^s}{\partial x}+\frac{i\omega\mu_0}{u^2}\frac{\partial H_y^s}{\partial z}\right)-\frac{i\omega\mu_0\Delta\sigma}{u^2}\hat{E}_x^p$$

$$\hat{E}_z^s=\left(\frac{i\omega\mu_0}{u^2}\frac{\partial H_y^s}{\partial x}-\frac{ik_y}{u^2}\frac{\partial\hat{E}_y^s}{\partial z}\right)-\frac{i\omega\mu_0\Delta\sigma}{u^2}\hat{E}_z^p$$

All these steps have to be repeated for each partial 2-D problem corresponding to each k_y of the Fourier transform. Since we use linear filter algorithm with 30 coefficients (Rijo & Almeida, 2003) to perform the Fourier transform, we have to run 30 times the 2-D partial finite element problem in order to obtain the final solution of the 2.5-D problem. This algorithm can easily be adapted to parallel computation. This is exactly what we are starting doing right now.